

# Computational Demonstrations of Density Wave of Cooper Pairs and Paired-Electron Liquid in the Quarter-Filled Band - a Brief Review

Sumit Mazumdar<sup>1</sup> and R. Torsten Clay<sup>2</sup>

<sup>1</sup>*Department of Physics, University of Arizona Tucson, AZ 85721*

<sup>2</sup>*Department of Physics and Astronomy and HPC<sup>2</sup> Center for Computational Sciences, Mississippi State University, Mississippi State MS 39762*

(\*Electronic mail: sumit@physics.arizona.edu)

(Dated: 25 June 2024)

There has been strong interest recently in the so-called Cooper pair density wave, subsequent to the proposition that such a state occurs in the hole-doped cuprate superconductors. As of now there is no convincing demonstration of such a state in the cuprate theoretical literature. We present here a brief but complete review of our theoretical and computational work on the paired-electron crystal (PEC), which has been also experimentally seen in the insulating phase proximate to superconductivity (SC) in organic charge-transfer solid (CTS) superconductors. Within our theory, SC in the CTS does indeed evolve from the PEC. A crucial requirement for the finding of the PEC is that the proper carrier density of one charge carrier per two sites is taken into consideration at the outset. Following the discussion of CTS superconductors, we briefly discuss how the theory can be extended to understand the phase diagram of the cuprate superconductors that has remained mysterious after nearly four decades of the discovery of SC in this family.

**Despite more than 30 years of research, the mechanism of superconductivity (SC) in the high- $T_c$  cuprates and other unconventional superconductors is still not understood. In a conventional superconductor the superconducting state evolves from a metal. However, in the cuprates and many other unconventional superconductors, unusual insulating phases are instead found adjacent to SC. In this paper we review theoretical work on one of these insulating phases, the Paired Electron Crystal (PEC). The PEC has been found experimentally in crystalline molecular superconductors known as organic charge-transfer solids. We describe theoretical work showing how SC can evolve from the PEC, and further how the PEC concept can be extended to understand the phase diagram of the high  $T_c$  cuprates.**

## I. INTRODUCTION

The theory of charge-density waves (CDWs), driven by either the Peierls intersite<sup>1</sup> or by the Holstein intrasite<sup>2</sup> electron-phonon (e-p) interactions in molecular solids are both quite old and well understood by now. The same is true with the concept of the Wigner crystal (WC), driven by intersite electron-electron (e-e) interactions<sup>3</sup>. In all such cases the electronic wavefunction in the ground state is characterized by periodic modulation of single electron densities. Should SC occur in such systems, the understanding has been that the driving force is once again the e-p interaction as in the traditional BCS theory<sup>4</sup>. Over the past several decades a different phenomenology, characteristic of many if not most unconventional superconductors, has attracted significant attention. This is the appearance of SC not merely proximate to CDW or spin-density wave (SDW)/antiferromagnetism (AFM) in the phase diagram, but the observation of actual “positive correlation” between spatial broken symmetry and SC, in that the SC may be evolving from the spatial broken symmetry state.

Evolution of SC from CDW broken state is in principle

likely if the CDW is “paired”, in that the electronic wavefunction exhibits modulation of pairs of charge carriers coupled into spin-singlets, as opposed to single electrons or holes. We have referred to this state as the PEC<sup>5,6</sup>, a terminology that existed prior to our work<sup>7</sup>. Conceptually it is possible to visualize SC emerging from the PEC with increasing lattice frustration or doping that leaves the paired singlets intact even as they become mobile. While this idea does not necessarily solve the problem of correlated-electron SC (which requires explicit demonstration of the transition from the PEC to the state with long-range superconducting pair-pair correlations), it does give an understandable starting point that has the added benefit of being “visual”.

We present here a brief review of our computational work, and show how the results can be used to understand spatial broken symmetries (especially CDW correlations) in organic CTS that are structurally related to CTS superconductors, or in the superconductors themselves in the normal state proximate to SC. We further discuss how the same concepts probably can be extended to understand hole as well as electron-doped cuprates. It is relevant in this context to note that the experimentally observed charge ordering in cuprates has been claimed to be a density wave of Cooper pairs by some research groups<sup>8–10</sup>. Computational results performed by our groups have demonstrated explicitly the occurrences of the PEC within a correlated-electron Hamiltonian on various lattices. The essential requirement is commensurability, which in turn occurs at strictly one particular carrier density. We will also discuss the possibility that moving away from strict commensurability can lead to SC, or at least a paired-electron liquid (PEL).

## II. THEORETICAL MODEL

The theoretical model we will consider is the same for all dimensionalities, the extended Hubbard Hamiltonian with nonzero intersite Coulomb repulsion and intersite Peierls and

intrasite Holstein e-p couplings,

$$H = - \sum_{\mathbf{v}, \langle ij \rangle_{\mathbf{v}}} t_{\mathbf{v}} (1 + \alpha_{\mathbf{v}} \Delta_{ij}) B_{ij} + \frac{1}{2} \sum_{\mathbf{v}, \langle ij \rangle_{\mathbf{v}}} K_{\alpha}^{\mathbf{v}} \Delta_{ij}^2 + g \sum_i v_i n_i + \frac{K_g}{2} \sum_i v_i^2 + U \sum_i n_{i\uparrow} n_{i\downarrow} + \frac{1}{2} \sum_{\langle ij \rangle} V_{ij} n_i n_j \quad (1)$$

In Eq. 1,  $\mathbf{v}$  runs over multiple lattice directions  $a$ ,  $b$  and  $c$ .  $B_{ij} = \sum_{\sigma} (c_{i\sigma}^{\dagger} c_{j\sigma} + H.c.)$ ,  $\alpha_{\mathbf{v}}$  is the intersite e-p coupling,  $K_{\alpha}^{\mathbf{v}}$  is the corresponding spring constant, and  $\Delta_{ij}$  is the distortion of the  $i$ - $j$  bond, to be determined self-consistently;  $v_i$  is the intrasite phonon coordinate and  $g$  is the intrasite e-p coupling with the corresponding spring constant  $K_g$ . The hoppings  $t_{\mathbf{v}}$  and intersite Coulomb interaction  $V_{ij}$  are between nearest neighbors (n.n). We consider only  $\rho = \frac{1}{2}$ , where there is strongest likelihood of commensurability-driven density wave composed of electron pairs. Additionally, much of our original motivation behind this research came from trying to reach a consistent theory of SC in organic CTS, which have uniformly carrier density per molecule of  $\rho = \frac{1}{2}$ .

### III. PEC IN ONE DIMENSION

#### A. Experimental Summary

Our involvement in this research area began with our attempt to understand the  $4k_F$  metal-insulator (M-I) and  $2k_F$  insulator (I-I) transitions in the organic CTS MEM(TCNQ)<sub>2</sub>, which at the time was understood the most experimentally. Each MEM donor molecule donates one electron to two TCNQ acceptor molecules, such that the one-dimensional (1D) stack of TCNQ anions has a carrier density  $\rho = \frac{1}{2}$  and is conducting at high temperatures in spite of large Hubbard intramolecular repulsion. Below 335 K the system undergoes M-I transition that is driven by intrastack bond dimerization<sup>11,12</sup>. At still lower temperature of 17.2 K there occur both bond and intramolecular site charge tetramerization<sup>11,12</sup> and a gap in the magnetic spectrum is observed from measurements of magnetic susceptibility<sup>12</sup>. Very similar coexisting bond and charge modulations were seen also in the low temperature tetramerized phase of TEA(TCNQ)<sub>2</sub>, which is insulating and dimerized already at high T<sup>13,14</sup>. Coexisting bond and charge-modulations had also been found in the so-called spin-Peierls (SP) phase of the cationic CT compounds (TMTTF)<sub>2</sub>PF<sub>6</sub> and (TMTTF)<sub>2</sub>AsF<sub>6</sub>, in which the charge on the TMTTF cation is  $\frac{1}{2}$ . The *coexisting* bond and charge tetramerization was not understood at the time.

It is important to understand in this context precisely *why* this coexistence was difficult to understand within what then was the traditional approach. Within the strongly correlated scenario the M-I transition in  $\rho = \frac{1}{2}$  is due either to  $4k_F$  bond dimerization (alternate short and long bonds) or to  $4k_F$  charge dimerization that results in the WC with alternate charge-rich and charge-poor sites. Within existing theories at the time,

each dimer in the bond-dimerized phase was considered as a single ‘‘site’’, the system was considered as an *effective* half-filled band (effective  $\rho = 1$ ), and bond tetramerization was the dimerization within this effective half-filled band. Charge and bond order modulations are not expected to coexist within the half-filled band<sup>15</sup>. Starting from the  $4k_F$  WC with alternate sites occupied by charge carrier, conversely, further bond dimerization would require unusually strong e-p couplings that could modulate the distances between ‘‘occupied’’ sites two lattice constants apart, making the bond tetramerization highly unlikely. Furthermore, the expected pattern of the bond distortion in this case, strong-strong-weak-weak, has not been observed in any CTS. The experimentally observed bond distortion pattern is strong-weak-strong-weak', with weak and weak' bond strengths different. In what follows we will find that precise understanding requires discarding the effective half-filled band concept at the outset.

#### B. Theory and Computational results.

As has been discussed extensively elsewhere<sup>16</sup>, physical insight to unconditional broken symmetries within Eq. 1 can be obtained by considering the limit of zero e-p coupling. In this limit and for  $U \rightarrow \infty$  the Hamiltonian in 1D reduces to the spinless Fermion Hamiltonian,

$$H_{\text{eff}} = V \sum_i n_i n_{i+1} - t \sum_i (a_i^{\dagger} a_{i+1} + a_{i+1}^{\dagger} a_i) \quad (2)$$

where  $a_i^{\dagger}$  create spinless Fermions and  $n_i = 0, 1$  only. For large  $V$ , the ground state now is the  $4k_F$  charge-ordered phase (CO)  $\dots 1010\dots$ , where the numbers 1 and 0 refer to actual site occupancies of  $0.5+\delta$  and  $0.5-\delta$ , respectively. It is essential here to appreciate that the WC is obtained only for  $V = V_c \geq 2|t|$ <sup>17</sup>. More importantly in the present case, extensive numerical calculations by multiple groups have that  $V_c$  *increases* as  $U$  becomes finite (for e.g.,  $V_c$  approaches  $3|t|$  at  $U = 8|t|$ )<sup>18-20</sup> The pertinent question is then what spatial broken symmetry occurs for  $V < V_c$ .

A conceptual framework that allows a pictorial resolution of this question is as follows. Consider a single dimer of two sites with one electron. The electron populations per site are 0.5 each, but the quantum mechanical wave function for the system is the superposition  $2^{-1/2}[10 + 01]$ , where 1 and 0 are site charge densities. If one now brings two of these dimers together, as in inset (a) of Fig. 1, the composite wave function of the two-dimer system can be written as  $\frac{1}{2}[1010 + 1001 + 0110 + 0101]$ . If the two electrons are in a spin-singlet state then within the simple Hubbard Hamiltonian the configuration 0110, in which singlet stabilization can occur from a single n.n. hop that creates a virtual double occupancy, must dominate over the configurations 1010 and 1001, in which singlet stabilization requires two and three hops, respectively. Thus as the singlet bond between the dimers gets stronger we expect increasing charge difference  $\delta$  between sites belonging to the same dimer (between sites 1 and 2, or between sites 3 and 4 in the linear chain of Fig. 1). Our proposed picture demands that similar charge disproportionation

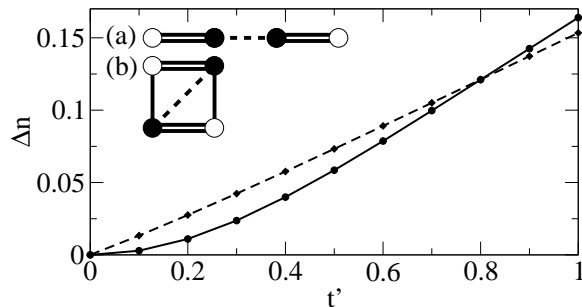


FIG. 1. Charge difference  $\Delta n$  versus hopping integral  $t'$  for two four-site systems. Solid lines are for the linear four-site system shown in inset (a); dashed lines are for the square plaquette in inset (b). Coulomb interactions are  $U = 4$  and  $V = 0$ . Double, single, and dashed lines represent hopping integrals of strengths  $t_1=1.5$ ,  $t_2=0.5$ , and  $t'$ , respectively. In the insets, filled and empty circles correspond to charge densities greater or less than 0.5. Reproduced from Ref. 6. Copyright 2011, American Physical Society.

occurs between members of the same dimer even in the case of the periodic molecule shown in the inset (b) of Fig. 1. In this case the charges on the sites connected by the diagonal bond must be larger than 0.5, while the charges on the two other sites must be smaller.

The conclusions drawn from the simple 4-atom calculations reported in Fig. 1 were confirmed from exact finite size calculations on  $N = 8, 12$  and  $16$  finite periodic rings<sup>21</sup>, and quantum Monte Carlo calculations<sup>22</sup> of up to  $N = 96$ . In all cases bond-order wave (BOW) and  $2k_F$  site-diagonal charge-density wave (CDW) coexist provided  $V < V_c$ . The results are summarized in Fig. 2. For noninteracting electrons or very small  $U$  the ground state broken symmetry consists of coexisting  $2k_F$  (period 4) BOW1 and  $2k_F$  CDW1, whereas for larger  $U$  the ground state is a superposition of a  $2k_F$  CDW2 and a BOW with the pattern strong-medium-weak-medium (SMWM) (2nd column of Fig. 2(a)). For stronger  $U$  and  $V$  the coexisting BOW instead has the pattern strong-weak-strong-weak' (SWSW', 4th column of Fig. 2(a)). The experimentally determined bond distortions and charge densities in MEM(TCNQ)<sub>2</sub><sup>12,21</sup> correspond exactly to this phase. The agreement with theory is true<sup>13,14</sup> also for the lowest temperature phases in TEA(TCNQ)<sub>2</sub>. Notice that the large charge densities in the BCDW1 and BCDW2 phases are coupled by spin-singlet bonds, and hence the CO phase does correspond to a density wave of spin singlets. The agreements are not surprising, and follow directly from the conceptual framework of Fig. 1, that is based only on the principle of charge-spin coupling in correlated  $\rho = \frac{1}{2}$  systems.

#### IV. THE WEAKLY TWO-DIMENSIONAL REGIME

##### A. Experimental Summary

The first organic superconductors, (TMTSF)<sub>2</sub>X, where X are monovalent anions PF<sub>6</sub><sup>-</sup>, AsF<sub>6</sub><sup>-</sup>, ClO<sub>4</sub><sup>-</sup> etc. were discovered in the early 1980s<sup>23</sup>. Unlike the TMTTF-based systems

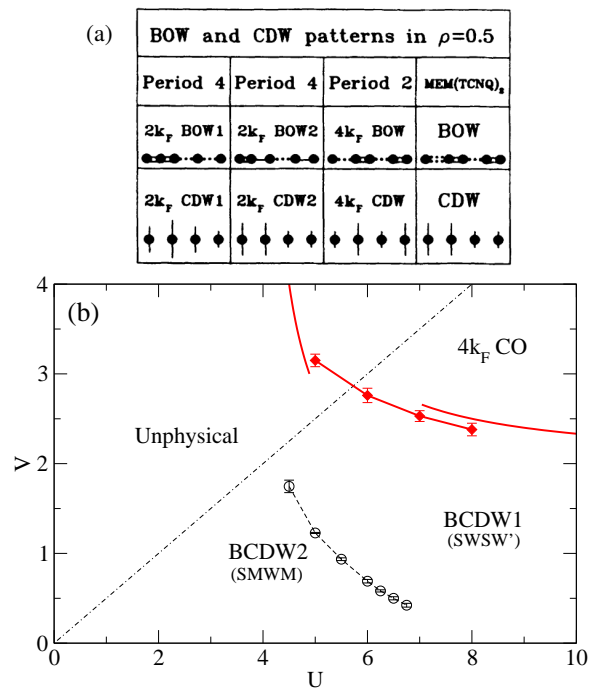


FIG. 2. (a) Schematic of the possible charge and bond distortions in a 1D chain with density 0.5. Single, double, and dotted lines represent undistorted, short, and long bonds, respectively. The length of the vertical lines corresponds to the charge density on each site. The last column shows the bond and charge distortions found in MEM(TCNQ)<sub>2</sub> at low temperature. Reproduced from Reference 21. Copyright 1994 American Physical Society. Zero temperature phase diagram of Eq. 1 in the limit of  $0^+$  electron-phonon interactions. BCDW2 is the  $2k_F$  BOW2 in (a); BCDW1 is the BOW shown in the 4th column of (a). The  $2k_F$  CDW1 of (a) only exists at very small  $U$  and is not shown here. The  $V = \frac{U}{2}$  line indicates the region of physical relevance for the organic CTS. Reproduced from Reference 22. Copyright 2017 American Physical Society.

which are quasi-one dimensional with spin-Peierls ground states, their Se analogues should be considered weakly two-dimensional (see below). The compound (TMTSF)<sub>2</sub>PF<sub>6</sub> has been studied the most intensively, and is considered the prototype member of this family. This compound exhibits metallic behavior at high temperature, but under ambient pressure there occurs transition to an incommensurate SDW at 12.5 K. The occurrence of the SDW, instead of the SP state, is direct evidence for non-negligible two-dimensional hopping between the TMTSF cations. Computations lead to parametrizations  $t_{\parallel} = 0.1-0.2$  eV,  $t_{\perp} = 0.01-0.02$  eV, where  $t_{\parallel}$  and  $t_{\perp}$  are the intra- and interstack hole hopping integrals between the TMTSF cations. Application of moderate pressure (6.5 kbar) leads to an apparent SDW-to-SC transition, with critical temperature  $T_c = 1.2$  K. Several other TMTSF compounds exhibit similar SDW-to-SC transitions. These observations had led to early applications of the spin-fluctuation theory of SC to this family of CT solids, as discussed below.

The intrastack intermolecular distances in (TMTSF)<sub>2</sub>X once again alternate and exhibit dimerization. Assumption of equal charge densities on the individual molecular sites within

each dimer then leads naturally to the effective  $\rho = 1$  description for  $(\text{TMTSF})_2\text{X}$  (as in  $(\text{TMTTF})_2\text{X}$ ), with the difference that interstack couplings are now non-negligible. The ground state is then a 2D commensurate  $\rho = 1$  AFM. Within this picture the superconducting transition is from AFM-to-SC, to be understood within the spin-fluctuation mechanism.

The above theoretical scenario was shown to be overly simplistic based on X-ray scattering experiments performed by Pouget and Ravy in 1997<sup>24</sup>. These authors found that the broken symmetry state in  $(\text{TMTSF})_2\text{PF}_6$  was a coexisting CDW-SDW state, which should not occur in true  $\rho = 1$ . Even more importantly, while a coexisting CDW-SDW state can be expected within the then standard WC models of strongly correlated  $\rho = \frac{1}{2}$ , the periodicities of CDW and SDW in this latter case are expected to be  $4k_F$  (alternate sites occupied by holes) and  $2k_F$  (opposite spins on n.n. occupied sites), respectively. The X-ray scattering measurement indicated *identical*  $2k_F$  periodicity (period 4) for both the CDW and the SDW. Pouget and Ravy labeled this broken symmetry “unprecedented”. Importantly, transition to a commensurate SDW was also found<sup>25</sup>. SC evolves from the coupled  $2k_F$  CDW-SDW and its mechanism has to be understood within this context.

## B. Theory and Computational results.

The physical arguments above for unequal intradimer charge occupancies in the 1D limit applies also to the weakly 2D antiferromagnetic case, as the stabilization of the antiferromagnet (over high spin states) originates also from virtual CT that creates double occupancies. Thus neighboring interdimer sites with shorter interdimer separation (stronger interdimer coupling) must have charge densities larger than corresponding interdimer site pairs with longer interdimer separation. This was proved within Eq. 1 from both 1D and 2D numerical calculations<sup>26</sup>. The 1D calculation involved adding external  $2k_F$  AFM potential to the static version of Hamiltonian 1, for fixed  $U$  and  $V$ , and determining the tendency to  $2k_F$  bond-charge distortion as a function of the strength of the AFM potential. The energy gained upon bond distortion increases with the strength of the external AFM potential, which is an indicator *co-operative coexistence* of  $2k_F$  BOW-CDW and  $2k_F$  AFM. The 2D calculations were done using the constrained path renormalization group (CPMC) approach for 4 coupled chains of length 12 sites each, periodic along both directions, with  $t_{\perp} = 0.1t_{\parallel}$ . Lowest ground state energy was found for  $\pi$ -phase difference between BOWs on neighboring chains, which was therefore adopted. Measurements of charge-charge and spin-spin correlations then established the coexisting  $2k_F$  CDW-SDW shown in Fig. 3. Once again there is charge disproportionation within each dimer unit cell, and the CDW is period 4. The coexisting  $2k_F$  SDW results from fractional charges within the dimer unit cell having the same spin, which is necessarily true as they together constitute a single hole. As in the 1D limit, the density wave of Fig. 3 is also paired, with the pair now being antiferromagnetically coupled as opposed to being spin singlet. It is then not inconceivable that as these pairs begin hopping between chains

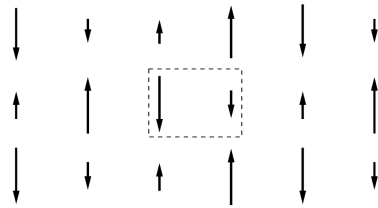


FIG. 3. The  $2k_F$  period 4 coexisting CDW-SDW found at  $\rho=0.5$ . The length of the arrows corresponds to the charge density on each site. The dashed box surrounds one dimer unit. Reproduced from Reference 26. Copyright 1999 American Physical Society.

with pressure-induced increase in  $t_{\perp}$  a superconducting state is reached.

## V. THE STRONGLY TWO-DIMENSIONAL REGIME

### A. Experimental Summary

The 2D CTS feature a great variety of compounds and behavior. There exist multiple recent reviews covering these systems<sup>16,27,28</sup>. Here we limit ourselves to only those discussions that pertain to the PEC. As with the weakly 2D superconducting CTS, these are also mostly 2:1 systems with general chemical formula  $\text{A}_2\text{X}$ , where A is the organic molecular component and X are inorganic monomer with charge  $-1$ , so that the average charge on the organic cation is  $+\frac{1}{2}$ . There also exist anionic 1:2 superconductors, with now organic anion charge of  $-\frac{1}{2}$ . We limit ourselves to cationic 2:1 superconductors only, as the physics of the anionic compounds are very similar and can be understood within the same theoretical approach<sup>16</sup>.

The largest number of 2D superconducting CTS have  $\text{A} = (\text{BEDT-TTF})$ , hereafter ET. While there exist other superconducting  $\text{A}_2\text{X}$  with cationic component different from ET, because of the limited scope of this presentation in what follows we limit ourselves to  $\text{A} = \text{ET}$  only, as these exhibit the full range of behavior seen in the 2:1 cationic superconductors.  $(\text{ET})_2\text{X}$  occur in different crystalline forms, which are labeled as  $\kappa$ ,  $\alpha$ ,  $\beta$  and  $\theta$ . In the following we give broad summaries of the experimental observations for each of these crystal structures.

**$\kappa$ -(ET) $_2$ X** These ET compounds with  $\text{X} = \text{Cu}(\text{NCS})_2$ ,  $\text{Cu}[\text{N}(\text{CN})_2]\text{Cl}$ ,  $\text{Cu}[\text{N}(\text{CN})_2]\text{Br}$ ,  $\text{Cu}_2(\text{CN})_3$  etc. have been among the most intensively studied CTS superconductors. The cation layer is characterized by strongly dimerized anisotropic triangular lattices with one hole per  $\text{ET}_2^+$  dimer. Relatively few have ground states that are AFM or quantum spin liquid (QSL), but much of the theoretical attention have centered around these, because of SC being proximate to these magnetic states, thus providing an apparently tangible connection to the observation in the cuprates. The other  $\kappa$ -phase materials exhibit CO or spin gap (SG). SG has been observed in some charge-ordered  $\kappa$ -(ET) $_2$ X. SC is spin-singlet, and the order parameter has nodes. There is evidence for intra-dimer

charge fluctuations and relatively strong lattice effects.

**$\beta$ -(ET) $_2$ X** These contain strongly interacting one-dimensional cation stacks, with the molecular planes nearly perpendicular to the stacking axes. Some of these exhibit ambient pressure SC, which is often proximate to nonmagnetic insulating states with pronounced lattice distortion that is often period-4. Others exhibit transition to SC under pressure. CO-to-SC transition is common among  $\beta$ -(ET) $_2$ X. In all cases where the pattern of the CO or bond distortion is known, they appear to be different from that of the simple WC, in that in more than one direction the CO pattern is  $\cdots 1100 \cdots$ . SG often accompanies the CO at the lowest temperatures.

**$\theta$ -(ET) $_2$ X** In the  $\theta$  structure molecules in neighboring stacks are tilted with respect to each other by dihedral angle  $100^\circ$ - $140^\circ$ . MI transition to CO is common to  $\theta$ -ET and is often followed by a lower temperature transition to a nonmagnetic state with SG. The CO consists of a stripe pattern (“horizontal”) which is different from a simple WC and has charge occupancies  $\cdots 1100 \cdots$  along the two most strongly coupled directions. SC occurs in  $X = I_3$ .

**$\alpha$ -(ET) $_2$ X** The  $\alpha$  structure is nearly identical to the  $\theta$  structure with the difference that the periodicity is doubled already in the room-temperature structure in the stacking direction by a weak dimerization. In addition, the stacks are often inequivalent. CO is common, with the CO pattern corresponding to horizontal stripe. CO and SG transitions occur at the same temperature in  $X = I_3$ . In some compounds there likely is co-existing CDW-SDW.

## B. Theory and Computational Results

The goal of the theoretical work here was to demonstrate geometrical lattice frustration-driven AFM-to-PEC transition, which we believe precedes the transition to SC in systems where apparently AFM and SC are proximate. Calculations were done starting from the bond dimerized limit along the  $x$ -direction, since (a) bond dimerization is essential to obtain AFM in  $\rho = \frac{1}{2}$ , and (b) CTS with AFM ground states are universally dimerized (see discussion on AFM in  $\kappa$ -(ET) $_2$ X above). The calculations were done on the  $4 \times 4$  lattice with both zero e-p interaction and externally imposed rigid dimerization (see Fig. 4(a)), as well as with nonzero e-p interactions along the  $x$  and  $y$  directions (see Fig. 4(b)). In the first case we chose periodic hoppings along the  $x$  and  $y$  directions but open boundary condition (OBC) along the  $x - y$  direction. The parameters for the OBC calculations were  $t_x = t \pm \delta_t$ ,  $t_y = t$ ,  $t = 1$ ,  $\delta_t = 0.2$ ,  $\alpha_v = g = 0$ , with in-phase bond dimerization between consecutive chains along the  $y$ -direction that gave commensurate AFM. In the second case all hoppings were periodic (periodic boundary condition, PBC) and e-p interactions were explicitly included. These latter parameters were  $\alpha_x = 1.3$ ,  $\alpha_y = 1.0$ ,  $\alpha_{x-y} = 0$ ,  $K_\alpha^x = K_\alpha^y = 2$ ,  $g = 0.1$  and  $K_g = 2$ . For the first set of calculations we report below we chose  $U = 4$ , and  $V_x = V_y = 1$ ,  $V_{x-y} = 0$ . The intersite Coulomb interactions were not large enough at the chosen  $U$  to give the WC ground state (note that nonzero  $V_{x-y}$  further destabilizes the WC). The parameter  $t_{x-y} = t'$  is the variable

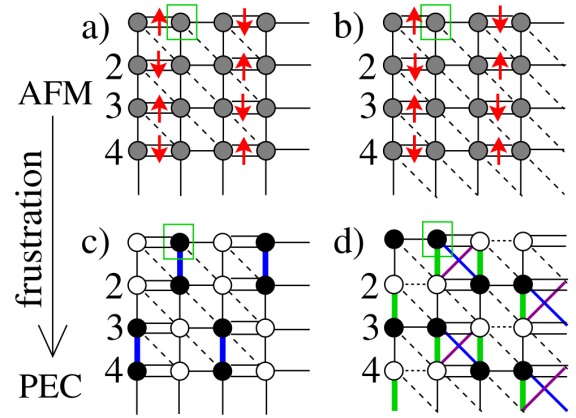


FIG. 4. Schematic of the AFM and PEC states as seen in a  $4 \times 4$  lattice. The hopping integral boundary conditions are periodic (PBC) along  $x$  and  $y$  directions in both (a) and (b) and open (OBC) and PBC in (a) and (b), respectively, along the  $x - y$  directions. Double and thick lines represent strong bonds; thin lines represent weak bonds. Dashed lines represent  $t'$ , whose strength is varied. Charge densities as indicated by grey circles are uniform in (a) and (b), and spin ordering corresponds to AFM. (c) and (d) shows the PEC state for  $t' > t'_c$ . Here black and white circles present charge-rich and charge-poor sites. Singlet bonds form between charge-rich sites. There occur periodic arrangement of spin-pairs along  $y$  and  $x - y$  directions in (a), and along  $x$  and  $x - y$  directions in (b). The box marks the reference site for spin-spin correlations shown in Fig. 5. Numbers are the chain indices used in Fig. 5(a) and (b). Reproduced from Reference 5. Copyright 2010 Institute of Physics Publishing.

that drives the AFM-PEC transition.

In Fig. 5(a) we show the  $z$ - $z$  spin-spin correlations for  $t' = 0$  between a fixed site (marked with box on each lattice in Fig. 4) and sites  $j$ , labeled sequentially 1, 2, 3, 4 from the left, on neighboring chains labeled 2, 3, 4 in Fig. 4. In Fig. 5(a) only, the average spin-spin correlation with each chain has been shifted to zero (note dotted line for  $\langle S_2^z S_j^z \rangle = 0$  in Figs. 5(a)-(b)) in order to clearly show the AFM pattern, which are  $\cdots - - + + \cdots$  and  $\cdots + + - - \cdots$  on the nearest and next nearest chains, indicating Néel ordering of the dimer spin moments in both lattices. The loss of this pattern in Fig. 5(b) for large  $t' = 0.7$  indicates loss of AFM order. In Fig. 5(c) we plot the spin-spin correlation between maximally separated dimers, which measures the strength of the AFM moment. This correlation is nearly constant until  $t' \sim 0.5$ , beyond which the AFM order is destroyed.

Fig. 5(d) shows the difference in charge densities  $\Delta n$  as a function of  $t'$ . There is a rapid increase in  $\Delta n$ , starting from zero, for  $t' > t'_c$  with both lattices. Simultaneously with CO, there is a jump in the bond orders  $\langle B_{ij} \rangle$  between the sites that form the localized spin-singlets. This is shown in Fig. 5(e). These bond orders are by far the strongest in both lattices for  $t' > t'_c$ . The spin-spin correlation between the same pairs of sites becomes strongly negative at the same  $t'$ , even as all other spin-spin correlations approach zero (Fig. 5(b)), indicating spin-singlet character of the strongest bonds. The simultaneous jumps in  $\langle S_i^z S_{i+R}^z \rangle$ ,  $\Delta n$  and  $\langle B_{ij} \rangle$  at the same  $t'$

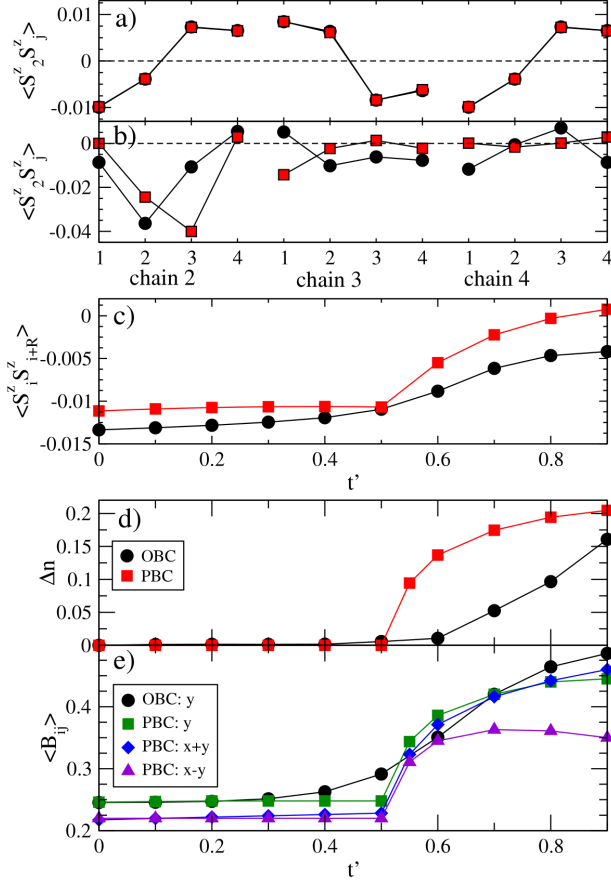


FIG. 5. (a) Spin-spin correlations  $\langle S_i^z S_j^z \rangle$  between site 2 (marked with a box in Fig. 4) and sites 1–4 in chains 2–4 for  $t'=0$ . In all panels, circles and squares correspond to OBC and PBC calculations, respectively. (b) Spin-spin correlations as in (a), but with  $t'=0.7$ . (c) Spin-spin correlations between sites of the most distant dimers versus  $t'$  (d) Charge disproportionation versus  $t'$  (e) Bond orders between pairs of n.n. sites forming localized spin-singlets. For the OBC these are along the  $y$  direction (see Fig. 4(c)). For the PBC lattice bonds along the  $y$ ,  $x+y$ , and  $x-y$  all change at the PEC transition (Fig. 4(d)). These are plotted using squares, diamonds, and triangles, respectively. Reproduced from Reference 5. Copyright 2010 Institute of Physics Publishing.

give conclusive evidence for the AFM-PEC transition shown in Fig. 4.

Fig. 6 shows how e-e interactions  $U$  and  $V$  affect the PEC<sup>6</sup>. As shown in Fig. 6(a), increasing  $U$  moderately increases  $t'_c$ . The figure also shows the effect of the n.n. Coulomb interaction  $V$ . Here the phase diagram depends critically on the form assumed for  $\langle V_{ij} \rangle$ . With  $V_x = V_y = V$  but  $V' = 0$ , the WC is found for sufficiently strong  $V$ , along with a narrow region where it coexists with a SG. The very narrow width of the WC-SG phase in the figure indicates the small likelihood of the WC coexisting with SG in real materials. Equally importantly, most CTS lattices are partially triangular, and the assumption that  $V' = 0$  is not realistic. For  $V_x = V_y = V'$  the WC and the PEC have the same classical energies; as shown in Fig. 6(b) in this case the WC is completely replaced by the

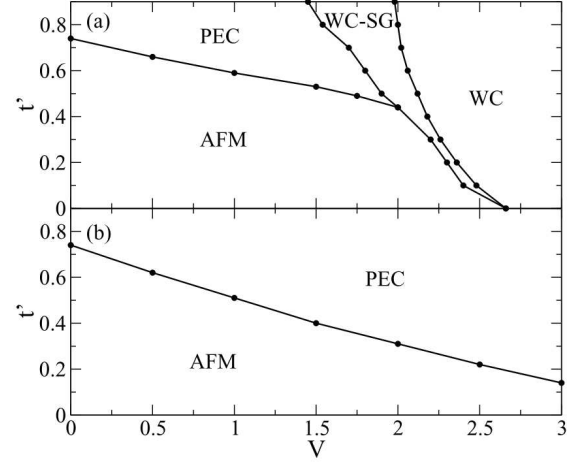


FIG. 6. (a) Phase diagram for the  $4 \times 4$  lattice of Fig. 4(b) as a function of  $t'$  and  $V = V_x = V_y$ ,  $V'=0$ , with  $U = 6$ ,  $\alpha_v=1.1$ ,  $g=0.1$ , and  $K_\alpha^v = K_g=2.0$ . (b) Same as (a), but with  $V = V_x = V_y = V'$ . Reproduced from Reference 6. Copyright 2011 American Physical Society.

PEC.

## VI. PEC AND SUPERCONDUCTING CORRELATIONS

To summarize the previous sections, the PEC is computationally arrived at  $\rho \simeq \frac{1}{2}$  independent of dimensionality, with geometric lattice frustration playing a key co-operative role. Experimentally, there is evidence for the PEC in many different families of CTS with 2:1 cation:anion composition ratio and in the few known 1:2 compounds that exhibit SC<sup>16</sup>. This is strong indication that SC evolves from the PEC following weak doping or increased frustration that lead to weak deviation from lattice commensurability. In the following we briefly review numerical results that support this viewpoint<sup>29</sup>.

Our calculations were within the static extended Hubbard Hamiltonian without e-p interactions,

$$H = - \sum_{(ij),\sigma} t_{ij} B_{i,j,\sigma} + U \sum_i n_{i,\uparrow} n_{i,\downarrow} + \frac{1}{2} \sum_{(ij)} V_{ij} n_i n_j \quad (3)$$

where all terms have the same meanings as in Eq. (1). Our calculations are for anisotropic triangular lattices with  $t_{ij} = t_x, t_y, t_{x+y}$ , periodic in all three directions. We express all quantities with dimensions of energy in units of  $t_x$  ( $t_x = 1$ ). The bulk of our calculations are for  $t_y = 0.9$  and  $t_{x+y}$  only slightly smaller than  $t_y$ . AFM or CO dominate at weaker frustrations, as seen in the previous sections. An essential condition for obtaining numerically precise results within the approximate quantum mechanical approaches used by us is having nondegenerate occupancies of single-particle levels in the noninteracting limit. The small inequalities between the hopping integrals maximizes the number of lattice sites  $N$  for which the ground state at or near quarter-filling is nondegenerate. used by us. With this constraint of nondegenerate ground states, and consideration of lattices for which  $L_y \geq L_x/2$ , our only

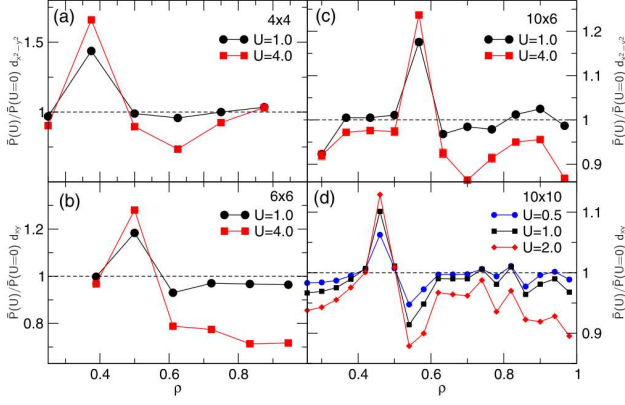


FIG. 7. Average long-range pair-pair correlation  $\bar{P}(U)$  normalized by its uncorrelated value for (a)  $4 \times 4$ , (b)  $6 \times 6$ , (c)  $10 \times 6$ , and (d)  $10 \times 10$  anisotropic triangular lattices, for  $t_y=0.9$  and  $t_{x+y}=0.8$ .  $4 \times 4$  results are exact;  $6 \times 6$  and  $10 \times 6$  results used the PIRG method; and  $10 \times 10$  the CPMC method. Reproduced from Reference 29. Copyright 2016 American Physical Society.

possible choices at the time these computations were done were  $10 \times 10$ ,  $10 \times 6$ , and  $6 \times 6$ . We considered the  $4 \times 4$  lattice in addition, which in spite of degeneracy at  $\rho = 0.5$  can be treated exactly.

We define the standard singlet pair-creation operators,

$$\Delta_i^\dagger = \sum_{\mathbf{v}} g(\mathbf{v}) \frac{1}{\sqrt{2}} (c_{i,\uparrow}^\dagger c_{i+\vec{r}_{\mathbf{v}},\downarrow}^\dagger - c_{i,\downarrow}^\dagger c_{i+\vec{r}_{\mathbf{v}},\uparrow}^\dagger), \quad (4)$$

For  $d_{x^2-y^2}$  symmetry,  $g(\mathbf{v}) = 1, -1, 1, -1$  for  $\vec{r}_{\mathbf{v}} = \hat{x}, \hat{y}, -\hat{x}, -\hat{y}$ , respectively. For  $d_{xy}$  symmetry,  $g(\mathbf{v}) = 1, -1, 1, -1$  for  $\vec{r}_{\mathbf{v}} = \hat{x} + \hat{y}, -\hat{x} + \hat{y}, -\hat{x} - \hat{y}, \hat{x} - \hat{y}$ , respectively. We calculated the distance-dependent pair-pair correlations  $P(r)$  ( $r \equiv |\vec{r}_i - \vec{r}_j|$ ) and show here the average long-range pair-pair correlation  $\bar{P} = N_P^{-1} \sum_{|\vec{r}| > 2} P(r)$ , where  $N_P$  is the number of terms in the sum<sup>30</sup>.

We found  $d_{x^2-y^2}$  and  $d_{xy}$  symmetries to dominate over  $s$ -wave symmetries. Further, for each lattice only one of the two  $d$ -wave channels is relevant;  $d_{x^2-y^2}$  for  $4 \times 4$  and  $10 \times 6$ , and  $d_{xy}$  for  $6 \times 6$  and  $10 \times 10$ . Note that the distinction between  $d_{x^2-y^2}$  and  $d_{xy}$  symmetries is largely semantic in the strongly frustrated regime we investigate. The complete results are summarized in Fig. 7. For each lattice  $\bar{P}(U)/\bar{P}(U=0) > 1$  for a single  $\rho$  that is either exactly 0.5 or one of two closest carrier fillings with closed-shell Fermi-level occupancy at  $U = 0$ . Pair correlations are *suppressed* by  $U$  at all other  $\rho$ , including the region  $0.7 < \rho < 1$  that has been extensively investigated in recent years. The unique behavior of  $\bar{P}(U)/\bar{P}(U=0)$  at or near  $\rho = 0.5$  cannot be merely coincidences, in view of what we have discussed in the previous sections.

Rigorous finite-size scaling of the pair-pair correlations is difficult, both because the enhancement of the pair-pair correlations occur for different symmetries ( $d_{x^2-y^2}$  versus  $d_{xy}$ ) as well as at slightly different densities for the different lattices. In Fig. 8 we have shown our attempt to finite-size scaling of  $\bar{P}$  at relatively small  $U$ . Long-range superconducting corre-

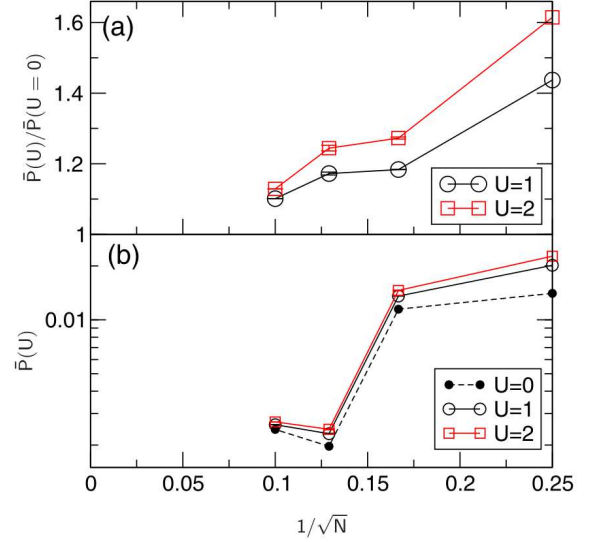


FIG. 8. Finite-size scaling of the  $\rho \approx 0.5$  peak of (a)  $\bar{P}(U)/\bar{P}(U=0)$  and (b)  $\bar{P}(U)$ .  $N$  is the total number of lattice sites. Reproduced from Reference 29. Copyright 2016 American Physical Society.

lations would require that  $\bar{P}$  to extrapolate to finite value as  $N \rightarrow \infty$ . This is clearly not the case as seen in Fig. 8(a). We point out, however, that if we ignore the data points for the largest lattice,  $10 \times 10$ ,  $\bar{P}(U)/\bar{P}(U=0)$  does converge to a nonzero value,  $\sim 0.2$ .

There are multiple possible interpretations of the apparent absence of long-range superconducting correlations. One possibility is that the state we are finding is a PEL that is asymptotically close to a superconducting state with long-range order. It is conceivable that phase coherence and long-range pairing is reached only upon inclusion of e-p interaction, but there should be no doubt that the state evolves from a PEC as commensurability effects are reduced.

Calculations similar to the above were done also for the  $\kappa$ -CTS lattice geometry<sup>31</sup>, with parameters corresponding to  $\kappa$ -(ET)<sub>2</sub>Cu[N(CN)<sub>2</sub>]Cl and  $\kappa$ -(ET)<sub>2</sub>Cu<sub>2</sub>(CN)<sub>3</sub> (hereafter  $\kappa$ -Cl and  $\kappa$ -CN, respectively), which have AFM and valence bond solid (VBS) ground states, respectively. The calculations were done for triangular dimerized lattices with 32 and 64 sites (where each site is an ET cation), with intra- and interdimer separations between sites and hopping integrals taken from the literature. Although the electron-concentration  $\rho_e$  in the ET cation in these compounds is fixed at 1.5, our calculations were for the full range of concentration  $1 < \rho_e < 2$ . We used the Path Integral Renormalization Group (PIRG) approach for all  $\rho_e$  for 32 sites and for  $\rho_e = 1.5$  for 64 sites. For the other densities on 64 sites we used the CPMC approach. We calculated both the spin-spin structure factor and superconducting pair-pair correlations with four different pairing symmetries, each close to being  $d$ -wave.

The calculated spin-spin structure factors at  $\rho_e = 1.5$  correctly predicted that  $\kappa$ -CN was further away from AFM than  $\kappa$ -Cl, but true long range AFM order was absent even for the latter in our calculations. We interpreted this to be in agree-

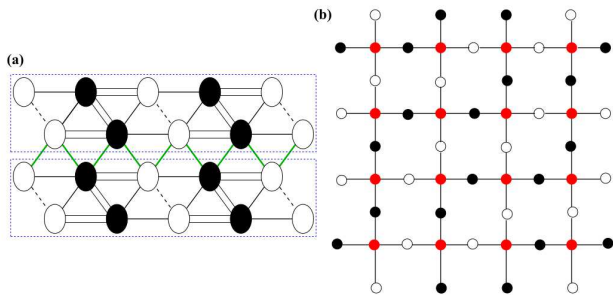


FIG. 9. (a) PEC charge order in the 2D  $\rho = \frac{1}{2}$  anisotropic triangular lattice. Filled and unfilled circles correspond to charge-rich and charge-poor sites; the strongest bonds are represented by double lines and the weakest by dotted lines. Filled circles connect by double lines are spin-singlet paired. Reproduced from Reference 29. Copyright 2016 American Physical Society. (b) Paired charge order in the checkerboard  $\frac{1}{4}$ -filled oxygen sublattice of the  $\text{CuO}_2$  plane following valence transition. The cations are uniformly  $\text{Cu}^{1+}$ . Migration of holes from the erstwhile  $\text{Cu}^{2+}$  ions generates the  $\rho \simeq \frac{1}{2}$  O-lattice. Filled and unfilled circles correspond to  $\text{O}^{1-}$  and  $\text{O}^{2-}$  ions, respectively. Pairs of  $\text{O}^{1-}$  ions linked by the same closed-shell  $\text{Cu}^{1+}$  will be spin-paired. The figure corresponds intertwined density waves with periodicities  $(2\pi/4a_0, 0)$  and  $(0, 2\pi/4a_0)$ . Reproduced from Reference 43. Copyright 2018 American Physical Society.

ment with the overall behavior of the  $\kappa$  family, within which relatively few have AFM ground states, with some members even exhibiting CO. The computational results, taken together with the experimental observations, are in broad agreement with our demonstration in Figs. 5 of the proximity in phase space between AFM and PEC. Our computational results of the superconducting pair-pair correlations were very similar to those in Fig. 7 for the triangular lattices: for both the  $\kappa$ -Cl and  $\kappa$ -CN lattices, and for both 32 and 64 sites the pair-pair correlations were enhanced by Hubbard  $U$  only for  $\rho_e$  exactly 1.5 or immediately proximate to this, for the same pairing symmetry<sup>31</sup>.

## VII. POSSIBLE APPLICATION OF THE PEC THEORY TO CUPRATE SUPERCONDUCTORS

Fully 36 years after the discovery of SC in the cuprates there is little progress towards understanding of this and related phenomena in these materials. Theoretical and computational investigations of cuprates have largely been within the single-band copper(Cu)-only Hubbard Hamiltonian, based on (a) the occurrence of commensurate AFM in the undoped semiconductors, and (b) the Zhang-Rice theory which claimed that the three-band description of the doped cuprates that does retain the oxygen (O)-ions can be reduced to the Cu-only one-band model<sup>32</sup>. This approach is encountering serious impasse. First, recent careful computational studies by many different groups have found absence of SC within the doped 2D Hubbard model with n.n. only hopping for carrier concentration 0.7 - 0.9<sup>33-35</sup>, as well as with more distant hoppings for the hole-doped case<sup>36,37</sup>. Our earlier results in Fig. 7 had found

the same absence of SC in this carrier concentration range. As of writing this problem has not been resolved. More importantly, the original Zhang-Rice work had not included the direct O-O hopping that characterizes real materials<sup>38</sup>. We have recently demonstrated the absence of quasi long-range superconducting correlations within the three-band Hamiltonian in the two-leg  $\text{Cu}_2\text{O}_3$  ladder<sup>39</sup>, in direct contradiction to theoretical results obtained within the one-band Hamiltonian for the two-leg ladder<sup>40,41</sup>. The strong inequivalence between one-band and three-band ladder results indicates the breakdown of the Zhang-Rice theory upon inclusion of direct O-O hopping<sup>39</sup>. There is no reason to believe that the validity of the theory will be restored upon going from the two-leg ladder to the 2D layer.

Beyond the above, satisfactory explanations of the spatial broken symmetries within the existing theoretical approaches have still not been reached. Experimental observations that continue to pose severe challenges include: (a) density wave of Cooper pairs<sup>8-10</sup> that we have already mentioned; (b) momentum space CO periodicity  $((Q, 0); (0, Q))$ , which is often interpreted as a quasi-1D stripe but in reality describes *intertwined orthogonal stripes*; (c) saturation with doping of  $Q$  to  $2\pi/4a_0$ , where  $a_0$  is the lattice constant, and finally, (d) simultaneous breaking of translational and  $C_4$  rotational symmetries, with the broken symmetry state characterized by inequivalency of O-ions belonging to the same  $\text{CuO}_2$  unit cell<sup>42</sup>. Each of these observations lie outside the scope of not merely the one-band Hubbard model but even the simple three-band model Hamiltonian. Theoretical and experimental developments, taken together, suggest that the fundamental assumptions that have gone into understanding SC in cuprates needs serious reexamination.

Simultaneous resolution to all of the above issues is reached within the dopant-induced valence-transition hypothesis that we have proposed for cuprates<sup>43,44</sup>, within which the PEC occurs naturally following the transition. The hypothesis is based on three separate but closely-related observations in transition metal oxides and heavy fermions that go beyond the concepts that have been used to understand cuprates until now. First, recent years have seen discoveries of *negative charge-transfer gap* in a large number of oxides and chalcogenides in which the true charge on the metal cation is  $M^{(n-1)+}$  with consequent *noninteger charge* on O-ions, instead of simple  $M^{n+}$  and  $\text{O}^{2-}$  as would be expected from the chemical formula. A partial list includes: (i)  $\text{BaBiO}_3$ , with Bi-ion charge uniformly 3+ (instead of alternating 3+ and 5+, as was believed until recently), (ii) rare-earth (RE) nickelates (RE) $\text{NiO}_3$  with  $\text{Ni}^{2+}$  (instead of  $\text{Ni}^{3+}$ ), (iii)  $\text{FeO}_2$  with  $\text{Fe}^{3+}$  (instead of  $\text{Fe}^{4+}$ ), (iv)  $\text{CrO}_2$  with  $\text{Cr}^{3+}$  (instead of  $\text{Cr}^{4+}$ ), (v)  $\text{AuTe}_2$  with  $\text{Au}^{1+}$ . etc. (see<sup>44</sup> for extended discussion and original citations). Second, as noted by us, in each of these cases  $M^{(n-1)+}$  electron occupancy is exactly closed-shell ( $d^{10}, t_{2g}^6$ ) or exactly  $\frac{1}{2}$ -filled ( $d^5, t_{2g}^3, e_g^2$ ) for the specific crystal structure, indicating that the  $M^{(n-1)+} \rightarrow M^{n+}$  ionization energy (I. E.) is higher than usual, a necessary condition for the system to have negative charge-transfer gap. This is where we further note that that the electron occupancy  $d^{10}$  of  $\text{Cu}^{1+}$  necessarily implies that the second I. E. of Cu ( $\text{Cu}^{1+} \rightarrow \text{Cu}^{2+}$ ) is unusually high

relative to the second I. E. of other 3d-elements<sup>43</sup>, indicating that cuprates are naturally very close to the boundary between positive and negative charge transfers. The third observation is that pressure- and temperature-driven transitions between different charge configurations that are close to the same boundary have been known in organic donor-acceptor charge-transfer complexes and heavy fermion compounds for over four decades (see<sup>44</sup> for complete discussions and citations). We therefore hypothesize that doping drives a similar valence transition in the layered cuprates, due to the reduced Madelung energy gain and greater O-hole bandwidth upon doping<sup>44</sup>.

The valence-transition hypothesis readily allows overcoming the difficulties within the existing models for cuprates. The closed-shell  $\text{Cu}^{1+}$  ions are now electronically inactive (exactly as the closed-shell  $\text{O}^{2-}$  ions are irrelevant in the undoped limit), and the hole density on the O-ions is nearly  $\frac{1}{2}$  in both electron- and hole-doped cuprates following the transition (since there are twice as many O-ions as Cu-ions). *Period 4 PEC of the holes on the O-ions is now a real possibility.* In Fig. 9 we have shown a schematic of the PEC proposed by us for the O-sublattice with hole charge-density  $\frac{1}{2}$ . We note that: (a) the spin-paired CO lacks  $C_4$  symmetry, thus explaining the simultaneous disappearance of translational and rotational symmetry (b) the PEC consists of criss-crossed stripes with periodicities  $(4a_0, 0)$  and  $(0, 4a_0)$ , as deduced from experiments. Computations are currently in progress to investigate whether or not such a paired CO occurs in the weakly doped  $\text{Cu}^{1+}\text{O}^{2-}\text{O}^{1-}$  lattice. These studies will be followed by search for the PEL state on the same lattice.

### VIII. CONCLUSIONS AND CONJECTURES

Spin-singlet formation is an essential step to reaching SC. The emergence of SC from the PEC can therefore be construed as a very natural phenomenon. In dimensionality greater than 1, however, the density wave must be commensurate. Carrier density at or near  $\rho = \frac{1}{2}$  leads naturally to commensurate PEC, which we have shown from accurate 2D correlated-electron calculations. Computations further indicate that only at or close to this density pair-correlations are enhanced by Hubbard  $U$ , yet another essential requirement for SC. Equally importantly, (a) SC in organic CTS is limited to  $\rho = \frac{1}{2}$ , even as nonsuperconductors with other carrier densities exist, and (b) the CO state proximate to SC, when they both occur, have been found to be the PEC. The idea that SC or PEL from the  $\rho = \frac{1}{2}$  PEC in the CTS thus appears to have a firm basis.

In the context of the cuprates the valence transition hypothesis, even as it is orthogonal to existing theories of cuprates, provides a strong starting point based on which the entire gamut of apparently contradictory observations can perhaps be explained. It is also relevant that there exists no alternate theoretical model currently that has either found long-range superconducting correlations, or has demonstrated a Cooper-pair density wave (we exclude here theoretical models that start from unrealistic parametrizations; for e.g., mod-

els which would give a spin-gapped state in the undoped limit rather than the experimentally observed commensurate AFM). We end this review by pointing out that very recent experimental works have claimed that even the strange metal phase in the cuprates evolves from the paired CO phase, and the charge carriers in this phase are Bosons<sup>45,46</sup>. Within our theory, the strange metal is a PEL. Observation of the strange metal state<sup>47</sup> proximate to the  $2k_F$  CDW-SDW state in  $(\text{TMTSF})_2\text{PF}_6$ , that we have shown to be a PEC (see Section IV.A), supports this viewpoint.

### ACKNOWLEDGMENTS

It is a pleasure to contribute this review paper to the special issue of Chaos dedicated to the 80th birthday of Professor David K. Campbell. David has been a mentor to and longtime collaborator of both of us. Mazumdar did his postdoctoral research under David's supervision at the Center for Nonlinear Studies, Los Alamos National Laboratory, where he was introduced to the fascinating topic of nonlinear excitations in organic conjugated polymers. Clay did his Ph.D. research under David's supervision in the Department of Physics, University of Illinois at Urbana-Champaign. Some of our earliest works on the paired-electron crystal, the topic of the present paper, were results of extended discussions and collaborations with David, that have continued over the years. We look forward to continued interactions with David on this and related topics. Earlier research reported here was supported in part by the NSF and U. S. Department of Energy. Recent work by SM is supported by NSF-DMR-2301372. Some of the calculations presented here were performed using the High Performance Computing resources supported by the University of Arizona and at Mississippi State University (MSU) in the MSU High Performance Computing Collaboratory (HPC<sup>2</sup>).

- <sup>1</sup>W. P. Su, J. R. Schrieffer, and A. J. Heeger, "Soliton excitations in polyacetylene," *Phys. Rev. B* **22**, 2099–2111 (1980).
- <sup>2</sup>T. Holstein, "Studies of polaron motion: Part I. the molecular-crystal model," *Ann. Phys.(N.Y.)* **8**, 325 (1959).
- <sup>3</sup>J. Hubbard, "Generalized Wigner lattices in one dimension and some applications to tetracyanoquinodimethane (TCNQ) salts," *Phys. Rev. B* **17**, 494–505 (1978).
- <sup>4</sup>J. Bardeen, L. N. Cooper, and J. R. Schrieffer, "Theory of superconductivity," *Phys. Rev. B* **108**, 1175–1204 (1957).
- <sup>5</sup>H. Li, R. T. Clay, and S. Mazumdar, "The paired-electron crystal in the two-dimensional frustrated quarter-filled band," *J. Phys.: Condens. Matter* **22**, 272201 (2010).
- <sup>6</sup>S. Dayal, R. T. Clay, H. Li, and S. Mazumdar, "Paired electron crystal: Order from frustration in the quarter-filled band," *Phys. Rev. B* **83**, 245106 (2011).
- <sup>7</sup>K. Mouloupoulos and N. W. Ashcroft, "New low density phase of interacting electrons: The paired electron crystal," *Phys. Rev. Lett.* **69**, 2555 (1992).
- <sup>8</sup>P. Cai *et al.*, "Visualizing the evolution from the Mott insulator to a charge-ordered insulator in lightly doped cuprates," *Proc. Natl. Acad. Sci.* **12**, 1047–1052 (2016).
- <sup>9</sup>M. H. Hamidian *et al.*, "Detection of a Cooper-pair density wave in  $\text{Bi}_2\text{Sr}_2\text{CaCu}_2\text{O}_{8+x}$ ," *Nature* **532**, 343–347 (2016).
- <sup>10</sup>A. Mesaros *et al.*, "Commensurate  $4a_0$ -period charge density modulations throughout the  $\text{Bi}_2\text{Sr}_2\text{CaCu}_2\text{O}_{8+x}$  pseudogap regime," *Proc. Natl. Acad. Sci.* **113**, 12661–12666 (2016).
- <sup>11</sup>R. J. J. Visser, S. Oostra, C. Vettier, and J. Voiron, "Determination of the spin-Peierls distortion in N-methyl-N-ethyl-morpholinium ditetra-

- cyanquinodimethanide [MEM(TCNQ)<sub>2</sub>]: Neutron diffraction study at 6 K,” *Phys. Rev. B* **28**, 2074–2077 (1983).
- <sup>12</sup>S. Huizinga, J. Kommandeur, G. A. Sawatzky, B. T. Thole, K. Kopinga, W. J. M. de Jonge, and J. Roos, “Spin-Peierls transition in N-methyl-N-ethyl-morpholinium-ditetra-cyanoquinodimethanide [MEM-(TCNQ)<sub>2</sub>],” *Phys. Rev. B* **19**, 4723–4732 (1979).
- <sup>13</sup>H. Kobayashi, Y. Ohashi, F. Marumo, and Y. Saito, “The crystal structure of tri-ethylammonium bis-7,7,8,8-tetra-cyanoquinodimethanide, (TEA)<sup>+</sup>(TCNQ)<sub>2</sub><sup>-</sup>,” *Acta. Cryst.* **B 26**, 459 (1970).
- <sup>14</sup>A. Filhol and M. Thomas, “Structural evolution of the one-dimensional organic conductor triethylammonium-7,7,8,8-tetracyano-p-quinodimethane (1:2) [TEA-(TCNQ)<sub>2</sub>] in the temperature range 40 to 345K,” *Acta. Cryst.* **B 40**, 44 (1984).
- <sup>15</sup>H. Q. Lin, D. K. Campbell, and R. T. Clay, “Phase diagram of the one dimensional extended Hubbard model,” *Chinese J. Phys.* **11**, 1 (2000).
- <sup>16</sup>R. T. Clay and S. Mazumdar, “From charge- and spin-ordering to superconductivity in the organic charge-transfer solids,” *Phys. Rep.* **788**, 1 (2019).
- <sup>17</sup>F. Mila and X. Zotos, “Phase diagram of the one-dimensional extended Hubbard model at quarter-filling,” *Europhys. Lett.* **24**, 133 (1993).
- <sup>18</sup>K. Penc and F. Mila, “Phase diagram of the one-dimensional extended Hubbard model with attractive and/or repulsive interactions at quarter filling,” *Phys. Rev. B* **49**, 9670–9678 (1994).
- <sup>19</sup>Y. Shibata, S. Nishimoto, and Y. Ohta, “Charge ordering in the one-dimensional extended Hubbard model: Implication to the TMTTF family of organic conductors,” *Phys. Rev. B* **64**, 235107 (2001).
- <sup>20</sup>R. T. Clay, S. Mazumdar, and D. K. Campbell, “The pattern of charge ordering in quasi-one dimensional organic charge-transfer solids,” *Phys. Rev. B* **67**, 115121 (2003).
- <sup>21</sup>K. C. Ung, S. Mazumdar, and D. Toussaint, “Metal-insulator and insulator-insulator transitions in the quarter-filled band organic conductors,” *Phys. Rev. Lett.* **73**, 2603–2606 (1994).
- <sup>22</sup>R. T. Clay, A. B. Ward, N. Gomes, and S. Mazumdar, “Bond patterns and charge order amplitude in  $\frac{1}{4}$ -filled charge-transfer solids,” *Phys. Rev. B* **95**, 125114 (2017).
- <sup>23</sup>D. Jérôme, A. Mazaud, M. Ribault, and K. Bechgaard, “Superconductivity in a synthetic organic conductor (TMTSF)<sub>2</sub>PF<sub>6</sub>,” *J. Phys. (Paris) Lett.* **41**, L95–L98 (1980).
- <sup>24</sup>J. P. Pouget and S. Ravy, “X-ray evidence of charge density wave modulations in the magnetic phases of (TMTSF)<sub>2</sub>PF<sub>6</sub> and (TMTTF)<sub>2</sub>Br,” *Synth. Metals* **85**, 1523 (1997).
- <sup>25</sup>S. Nagata, M. Misawa, Y. Ihara, and A. Kawamoto, “Commensurability of the spin-density-wave state of (TMTSF)<sub>2</sub>PF<sub>6</sub> observed by <sup>13</sup>C-NMR,” *Phys. Rev. Lett.* **110**, 167001 (2013).
- <sup>26</sup>S. Mazumdar, S. Ramasesha, R. T. Clay, and D. K. Campbell, “Theory of coexisting charge- and spin-density waves in (TMTTF)<sub>2</sub>Br, (TMTSF)<sub>2</sub>PF<sub>6</sub>, and  $\alpha$ -(BEDT-TTF)<sub>2</sub>MHg(SCN)<sub>4</sub>,” *Phys. Rev. Lett.* **82**, 1522–1525 (1999).
- <sup>27</sup>M. Dressel and S. Tomić, “Molecular quantum materials: electronic phases and charge dynamics in two-dimensional organic solids,” *Adv. Phys.* **69**, 1–120 (2020).
- <sup>28</sup>T. Naito, “Modern history of organic conductors: An overview,” *Crystals* **11**, 838 (2021).
- <sup>29</sup>N. Gomes, W. W. De Silva, T. Dutta, R. T. Clay, and S. Mazumdar, “Coulomb enhanced superconducting pair correlations in the frustrated quarter-filled band,” *Phys. Rev. B* **93**, 165110 (2016).
- <sup>30</sup>Z. B. Huang, H. Q. Lin, and J. E. Gubernatis, “Quantum Monte Carlo study of spin, charge, and pairing correlations in the  $t$ - $t'$ - $U$  Hubbard model,” *Phys. Rev. B* **64**, 205101 (2001).
- <sup>31</sup>W. De Silva, N. Gomes, S. Mazumdar, and R. T. Clay, “Coulomb enhancement of superconducting pair-pair correlations in a  $\frac{3}{4}$ -filled model for  $\kappa$ -(BEDT-TTF)<sub>2</sub>X,” *Phys. Rev. B* **93**, 205111 (2016).
- <sup>32</sup>F. C. Zhang and T. M. Rice, “Effective Hamiltonian for the superconducting Cu oxides,” *Phys. Rev. B* **37**, 3759(R)–3761(R) (1988).
- <sup>33</sup>S. Zhang, J. Carlson, and J. E. Gubernatis, “Pairing correlations in the two-dimensional Hubbard model,” *Phys. Rev. Lett.* **78**, 4486 (1997).
- <sup>34</sup>M. Qin, C.-M. Chung, H. Shi, E. Vitali, C. Hubig, U. Schollwöck, S. R. White, and S. Zhang, “Absence of superconductivity in the pure two-dimensional Hubbard model,” *Phys. Rev. X* **10**, 031016 (2020).
- <sup>35</sup>M.-S. Vaezi, A.-R. Negari, A. Moharramipour, and A. Vaezi, “Amelioration for the sign problem: an adiabatic quantum Monte Carlo algorithm,” *Phys. Rev. Lett.* **127**, 217003 (2021).
- <sup>36</sup>S. Jiang, D. J. Scalapino, and S. R. White, “Ground-state phase diagram of the  $t-t'-J$  model,” *Proceedings of the National Academy of Sciences of the USA* **118**, e2109978118 (2021).
- <sup>37</sup>S. Jiang, D. J. Scalapino, and S. R. White, “Pairing properties of the  $t$ - $t'$ - $t''$ - $J$  model,” *Phys. Rev. B* **106**, 174507 (2022).
- <sup>38</sup>M. Hirayama, Y. Yamaji, T. Misawa, and M. Imada, “Ab initio effective Hamiltonians for cuprate superconductors,” *Phys. Rev. B* **98**, 134501 (2018).
- <sup>39</sup>J.-P. Song, S. Mazumdar, and R. T. Clay, “Doping asymmetry in the three-band hamiltonian for cuprate ladders: Failure of the standard model of superconductivity in cuprates,” *Phys. Rev. B* **107**, L241008 (2023).
- <sup>40</sup>R. M. Noack, S. R. White, and D. J. Scalapino, “Correlations in a two-chain Hubbard model,” *Phys. Rev. Lett.* **73**, 882–885 (1994).
- <sup>41</sup>R. M. Noack, N. Bulut, D. J. Scalapino, and M. G. Zacher, “Enhanced  $d_{x^2-y^2}$  pairing correlations in the two-leg Hubbard ladder,” *Phys. Rev. B* **56**, 7162 (1997).
- <sup>42</sup>S. Mukhopadhyay, R. Sharma, C. K. Kim, S. D. Edkins, *et al.*, “Evidence for a vestigial nematic state in the cuprate pseudogap phase,” *Proc. Natl. Acad. Sci.* **116**, 13249–13254 (2019).
- <sup>43</sup>S. Mazumdar, “Valence transition model of the pseudogap, charge order, and superconductivity in electron-doped and hole-doped copper oxides,” *Phys. Rev. B* **98**, 205153 (2018).
- <sup>44</sup>J.-P. Song, R. T. Clay, and S. Mazumdar, “Valence transition theory of the pressure-induced dimensionality crossover in superconducting Sr<sub>14-x</sub>Ca<sub>x</sub>Cu<sub>24</sub>O<sub>41</sub>,” *Phys. Rev. B* **108**, 134510 (2023).
- <sup>45</sup>G. Seibold *et al.*, “Strange metal behaviour from charge density fluctuations in cuprates,” *Commun. Phys.* **4**, 1–6 (2021).
- <sup>46</sup>C. Yang *et al.*, “Signatures of a strange metal in a bosonic system,” *Nature* **601**, 205–210 (2022).
- <sup>47</sup>N. Doiron-Leyraud *et al.*, “Correlation between linear resistivity and  $T_c$  in the Bechgaard salts and the pnictide superconductor Ba(Fe<sub>1-x</sub>Co<sub>x</sub>)<sub>2</sub>As<sub>2</sub>,” *Phys. Rev. B* **80**, 214531 (2009).